SCIENCE CHINA
Physics, Mechanics & Astronomy

• Article •

July 2012 Vol.55 No.7: 1297–1306
doi: 10.1007/s11433-012-4741-6

Multipath error detection and correction for GEO/IGSO satellites†

WU XiaoLi[1,2], ZHOU JianHua[2*], WANG Gang[2], HU XiaoGong[1] & CAO YueLing[1]

[1] *Shanghai Astronomical Observatory, Chinese Academy of Sciences, Shanghai 200030, China;*
[2] *Beijing Global Information Application and Development Center, Beijing 100094, China*

Received August 20, 2011; accepted October 12, 2011; published online April 19, 2012

Constellations of regional satellite navigation systems are usually constituted of geostationary satellites (GEO) and inclined geostationary satellites (IGSO) for better service availability. Analysis of real data shows that the pseudorange measurements of these two types of satellites contain significant multipath errors and code noise, and the multipath for GEO is extremely serious, which is harmful to system services. In contrast, multipath error of carrier phase measurements is less than 3 cm, which is smaller than the multipath of pseudorange measurements by two orders of magnitude. Using a particular combination of pseudorange and dual-frequency carrier phase measurements, the pseudorange multipath errors are detected, and their time varying features are analyzed. A real-time multipath correction algorithm is proposed in this paper, which is called CNMC (Code Noise and Multipath Correction). The algorithm decreases the influence of the multipath error and therefore ensures the performance of the system. Data processing experiments show that the multipath error level may be reduced from 0.5 m to 0.15 m by using this algorithm, and 60% of GEO multipath errors and 42% of IGSO multipath errors are successfully corrected with CNMC. Positioning experiments are performed with a constellation of 3 GEO plus 3 IGSO satellites. For dual-frequency users the East-West position accuracy is improved from 1.31 m to 0.94 m by using the CNMC algorithm, the South-North position accuracy is improved from 2.62 m to 2.29 m, and the vertical position accuracy is improved from 4.25 m to 3.05 m. After correcting multipath errors, the three-dimensional position accuracy is improved from 5.16 m to 3.94 m.

multipath error, carrier smoothing pseudorange, GEO satellite, position error

PACS number(s): 95.75.Wx, 95.75.Pq, 94.20.Vv, 95.10.Eg

Citation: Wu X L, Zhou J H, Wang G, et al. Multipath error detection and correction for GEO/IGSO satellites. Sci China-Phys Mech Astron, 2012, 55: 1297–1306, doi: 10.1007/s11433-012-4741-6

With the increasingly wide applications of GNSS (Global Navigation Satellite System) and the continuous perfection of technologies, pseudorange multipath has become one of the major sources of error that influences positioning, navigation and timing services. When direct navigation signals arrive at a receiver antenna, the reflected and refracted indirect signals also arrive at the receiver antenna at the same time contaminating the direct signals. This phenomenon is called the multipath effect, and measurement errors caused by these indirect signals are multipath errors. Studies on GPS multipath effects have demonstrated that multipath not only distorts the pseudo-random noise code and navigation messages modulated on the navigation signals, but also distorts the carrier phase. Multipath error decreases the accuracy of ranging, as well as carrier phase and Doppler data, hence degrading the quality of measurements. The worst multipath effect may even result in the loss of the receiver tracking loop. Commonly used error processing techniques such as data modeling or differential treatments are not able to completely eliminate the error caused by the multipath effect [1].

As GEO satellites are stationary relative to receivers on the Earth, multipath errors of GEO are much more serious

*Corresponding author (email: Julianma@263.net.cn)
†Recommended by ZHOU JiLin (Associate Editor)

than that of IGSO or MEO. [2] indicates that an analysis periodically performed for each WAAS reference station shows that the multipath error is normally less than 1 meter with two or three stations exhibiting errors over 2 meters. An analysis performed for regional satellite navigation system indicates that pseudorange multipath errors vary significantly both in time and spatial domains for different stations, with some stations having multipath errors over 4 meters [1]. Multipath errors present a new challenge to provide high precision navigation services, and have become a limiting factor for system service performance improvement.

Theoretically, according to the multipath generation mechanism, multipath error of carrier phase measurements is about 1/4 of the wavelength or less, which is about 4–5 cm at the navigation L band, and the multipath error of carrier phase measurements is two orders of magnitude smaller than that of pseudorange measurements. After verifying this with tri-frequency measurements, we use a particular combination of pseudorange and dual-frequency carrier phase measurements to detect and separate the pseudorange multipath error, and then their time varying features are analyzed in this paper. A new real-time multipath correction algorithm is proposed and the correction effects are assessed. The validity of this multipath correction algorithm is proved by improvement of positioning accuracy.

1 Multipath error of pseudorange measurements

Following the basic navigation principles, a pseudorange measurement contains information of satellite orbit, satellite clock error, receiver position, receiver clock error, ionospheric delay, neutral atmosphere delay, multipath error and random noise(as shown in eq. (1)). In addition to phase ambiguity, a carrier phase measurement contains the same satellite orbit, satellite clock error, receiver position, receiver clock error, and neutral atmosphere delay with the pseudorange measurement. However, for the same frequency, the ionospheric delay of carrier phase measurements is opposite to that of pseudorange, which is about 1–2 cm ignoring the high-order ionospheric delay. Our reasoning is that if the multipath error of carrier phase measurements can be verified to be negligible compared to the pseudorange multipath, then the carrier phase measurements can be treated as a reference to detect and separate the multipath errors for each single frequency pseudorange measurement.

1.1 Multipath error of carrier phase measurements

It is impossible to separate the multipath error of a single frequency carrier phase measurement, so we estimate the carrier phase multipath magnitude by using three frequency navigation signals to calculate different carrier phase ionosphere-free combinations instead. Specifically, we first calculate the ionosphere-free combination LC12 using phase measurements at B1 and B2, and then calculate the ionosphere-free combination LC13 using phase measurements at B1 and B3. The difference between LC12 and LC13 should be nothing but the combination of ambiguity, random noise and possible multipath errors of carrier phases.

GNSS pseudorange and carrier phase observation equations are as follows:

$$P = \left|\boldsymbol{R}^{\mathrm{sat}} - \boldsymbol{R}_{\mathrm{rcv}}\right| + \Delta t_{\mathrm{rcvclk}} - \Delta t_{\mathrm{satclk}} + \Delta t_{\mathrm{trop}} + \Delta t_{\mathrm{iono}} + \Delta t_{\mathrm{cor}} + \tau_{\mathrm{sat}} + \tau_{\mathrm{rcv}} + M_{\mathrm{P}} + \varepsilon_{\mathrm{P}}, \quad (1)$$

$$\phi \cdot \lambda = \left|\boldsymbol{R}^{\mathrm{sat}} - \boldsymbol{R}_{\mathrm{rcv}}\right| + \Delta t_{\mathrm{rcvclk}} - \Delta t_{\mathrm{satclk}} + \Delta t_{\mathrm{trop}} - \Delta t_{\mathrm{iono}} + \Delta t_{\mathrm{cor}} + Amb_{\phi} + M_{\phi} + \varepsilon_{\phi}, \quad (2)$$

where $\boldsymbol{R}^{\mathrm{sat}}$ is the satellite position vector, $\boldsymbol{R}_{\mathrm{rcv}}$ is the receiver position vector, and Δt_{cor} is the correction of observation errors, including antenna phase center corrections of both the satellite and receiver, station eccentric corrections and tidal corrections. $\Delta t_{\mathrm{rcvclk}}$ is the receiver clock error, $\Delta t_{\mathrm{satclk}}$ is the satellite clock error, Δt_{trop} is the neutral atmosphere delay, Δt_{iono} is the ionospheric delay, and τ_{sat} and τ_{scv} are the payload-dependent or receiver-dependent time delays of the satellite and receiver. Amb_{ϕ} is the carrier phase ambiguity, M_{P} and ε_{P} are the multipath error and random noise of pseudorange measurements, and M_{ϕ} and ε_{ϕ} are the multipath error and random noise of carrier phase measurements.

GNSS pseudorange and carrier phase ionosphere-free observation equations are as follows:

$$PC = \left|\boldsymbol{R}^{\mathrm{sat}} - \boldsymbol{R}_{\mathrm{rcv}}\right| + \Delta t_{\mathrm{rcvclk}} - \Delta t_{\mathrm{satclk}} + \Delta t_{\mathrm{trop}} + \Delta t_{\mathrm{cor}} + M_{\mathrm{PC}} + \tau_{\mathrm{bias}}, \quad (3)$$

$$LC = \left|\boldsymbol{R}^{\mathrm{sat}} - \boldsymbol{R}_{\mathrm{rcv}}\right| + \Delta t_{\mathrm{rcvclk}} - \Delta t_{\mathrm{satclk}} + \Delta t_{\mathrm{trop}} + AMB_{\mathrm{LC}} + \Delta t_{\mathrm{cor}} + M_{\mathrm{LC}}, \quad (4)$$

where, M_{PC} is the pseudorange ionosphere-free combination, M_{LC} is the carrier phase ionosphere-free combination, AMB_{LC} is the ambiguity combination of carrier phase, and τ_{bias} is the hardware bias combination.

Using tri-frequency pseudorange and carrier phase measurements of China's Beidou navigation system, the difference between the B1-B2 ionosphere-free combination and the B1-B3 ionosphere-free combination is as follows:

$$difPC = PC_{12} - PC_{13} = M_{\mathrm{PC12}} - M_{\mathrm{PC13}} + \tau_{\mathrm{bias12}} - \tau_{\mathrm{bias13}}, \quad (5)$$

$$difLC = LC_{12} - LC_{13} = M_{\mathrm{LC12}} - M_{\mathrm{LC13}} + AMB_{\mathrm{LC12}} - AMB_{\mathrm{LC13}}. \quad (6)$$

Note the ionosphere-free measurement random noise is about 2 times that of the single frequency measurement according to error propagation.

The hardware bias of either the satellite or the receiver is assumed to be constant during an arc-length of 24 hours or shorter, so $\tau_{\text{bias12}}-\tau_{\text{bias13}}$ in eq. (5) is a constant. If there were no multipath errors of pseudorange measurements, the time series of *difPC* in eq. (5) would be white noise with zero mean after removing the hardware bias combinations. Since there is ambiguity on carrier phase measurements, *difLC* in eq. (6) contains the ambiguity combination of three frequency carrier phases. High-precision cycle slip detection is necessary to calculate the ambiguity of *difLC*.

If the difference of *difLC* between the previous and current epochs is larger than 0.5 m, which is equivalent to approximately one cycle slip, then there must be a cycle slip at a certain frequency, so the location of this cycle slip is flagged. The mean of *difLC* during the non-cycle slip period is the ambiguity combination of this period.

As an example, using three days of continuous measurements for a GEO satellite, we analyze the difference between the B1-B2 ionosphere-free combination and the B1-B3 ionosphere-free combination of carrier phase and pseudorange measurements (Figures 1(a) and (b) respectively). The elevation angle of this GEO satellite is 22 degrees. The left panel shows the *difLC* after removing the ambiguity combination (Figure 1(a)). The right panel shows the *difPC* after removing the hardware biases (Figure 1(b)). As shown in Figure 1(a), the peak-to-peak multipath error of the carrier phase combination is less than 3 cm with root-mean-squares (RMS) being 0.008 m. Meanwhile the peak-to-peak multipath error of the pseudorange combination is about 1.5 m, and the RMS is 0.549 m. It can be observed from the panels that there exists significant daily multipath error pattern repeatability both in pseudorange measurements and carrier phases. Experimental results have confirmed that this daily repeatability is the consequence of the GEO satellites geostationary characteristics.

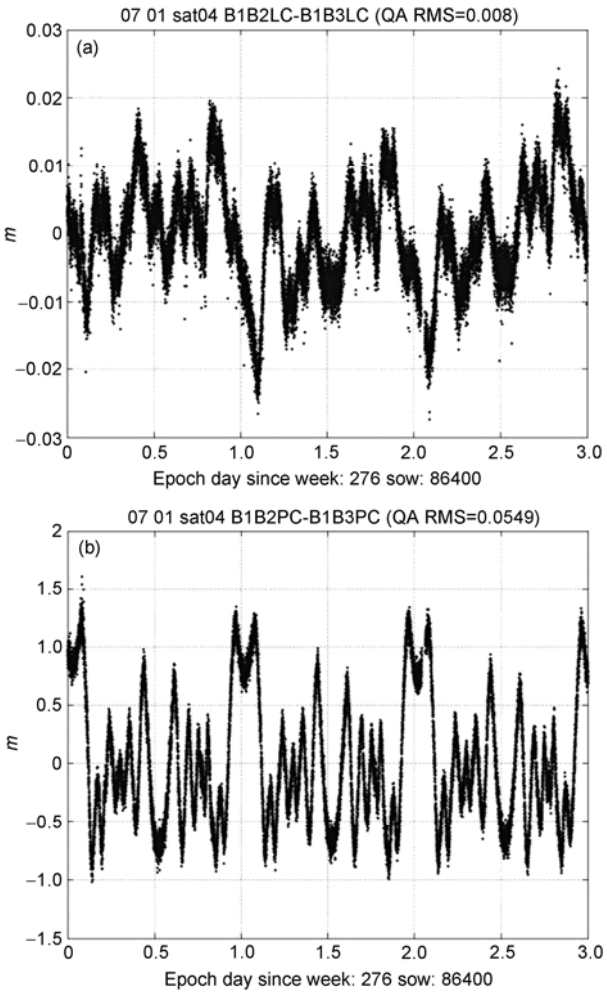

Figure 1 The horizontal axis represents observation time (unit: day) and the vertical axis represents the difference between the B1-B2 ionosphere-free combination and the B1-B3 ionosphere-free combination (unit: m). (a) M_{LC12}–M_{LC13}; (b) M_{PC12}–M_{PC13}.

1.2 Multipath error of pseudorange measurements

If carrier phase multipath error and random noise are ignored, by using the measurement combinations of pseudorange and carrier phase, the equations separating the pseudorange multipath error for a single frequency are as follows[3,4]:

$$\begin{aligned} M_{\text{P1}} &= P_1+\frac{1+\alpha_{12}}{1-\alpha_{12}}\phi_1\cdot\lambda_1-\frac{2}{1-\alpha_{12}}\phi_2\cdot\lambda_2,\\ M_{\text{P2}} &= P_2+\frac{2\alpha_{12}}{1-\alpha_{12}}\phi_1\cdot\lambda_1-\frac{1+\alpha_{12}}{1-\alpha_{12}}\phi_2\cdot\lambda_2,\\ M_{\text{P3}} &= P_3+\frac{2\alpha_{13}}{1-\alpha_{13}}\phi_1\cdot\lambda_1-\frac{1+\alpha_{13}}{1-\alpha_{13}}\phi_3\cdot\lambda_3, \end{aligned} \tag{7}$$

where, P_1, P_2, P_3 and ϕ_1, ϕ_2, ϕ_3 are B1, B2, B3 pseudorange measurements and carrier phase measurements respectively, λ_1, λ_2, λ_3 and f_1, f_2, f_3 are B1, B2, B3 wavelengths and frequencies, and $\alpha_{12}=\dfrac{f_1^2}{f_2^2}$, $\alpha_{13}=\dfrac{f_1^2}{f_3^2}$.

It is easy to verify that the equations above include the ambiguity combination, hardware bias combination, pseudorange multipath error and random noise, while eliminating the geometric distance between the satellite and the receiver, clock error, atmosphere delay and other delays specific for the receiver. After the ambiguity combination and hardware bias combination are calculated successfully and removed, M_{P} must be left with only multipath error and random noise .

By analyzing the real data using eq. (7), the error features of pseudorange measurements are summarized as follows:

(1) The error varies with satellite elevation angles and larger error is associated with a lower elevation angle.

(2) The error varies with the apparent movement between a satellite and a receiver. The GEO error shows larger magnitude with medium- and low-frequency fluctuations, while

the high-frequency fluctuations are shown in IGSO error.

(3) The error varies with code rates. With the use of a choke antenna, the error of high rate navigation signals is smaller than the error of low rate navigation signals.

(4) GEO satellite error shows significant daily repeatability patterns.

A series of field experiments indicate that these distinct features of system error discussed above are derived from the ground multipath effects of GEO/IGSO satellites [1].

According to eq. (7), the multipath error of three frequency pseudorange measurements for a GEO satellite are shown in Figure 2(a). As shown in the figure, the magnitude of multipath error at B1 is the largest with a peak value more than 1 m, and the multipath RMS is 0.68 m. The multipath peak values at B2 and B3 are about 0.5 m, and the RMS are about 0.2 m. The one-day time series of B2 or B3 multipath error contains smoother fluctuations. In contrast, B1 multipath error includes significant high-frequency fluctuations with time scales less than 0.5 hour. The multipath error of the ionosphere-free pseudorange combinations is shown in Figure 2(b). The peak values of multipath error of the ionosphere-free combinations are about 4 m, with a multipath RMS for the B1-B2 ionosphere-free combination of 1.71 m, and a multipath RMS for the B1-B3 ionosphere-free combination of 2.17 m. As can be seen from the figure, the multipath trend of the B1-B2 and B1-B3 ionosphere-free combination is similar.

Dual-frequency pseudorange combination is used to compute ionosphere vertical total electricity content (VTEC). The existing serious multipath has brought great errors into VTEC calculations. As a result VTEC obtained using dual-frequency pseudorange is quite different from true VTEC as measured by GPS for example. Furthermore, because of the differences in multipath error at each frequency, VTECs obtained with different frequency combinations are indeed inconsistent with each other. This inconsistency presents a new challenge for regional systems to provide high accuracy navigation services.

Shown in Figure 3 are different ionosphere zenith delays for a GEO satellite computed using different frequency combinations. Note that ionospheric delays caused by the same amount of VTEC are different for different frequencies. One TEC unit amount of VTEC is equivalent to a delay of approximately 0.25 m at B3. The red and green curves in Figure 3 represent the computed ionosphere VTEC using B1-B2 and B1-B3 pseudorange combinations respectively. The blue curve represents the ionosphere VTEC using a B1-B2 carrier phase combination after fixing the phase ambiguities. The black curve represents the ionosphere VTEC at the same IPP (ionospheric pierce point) using the GIM (global ionosphere map) model provided by IGS. As can be seen from Figure 3, the blue curve and the black curve agree well except for some details. We interpret the discrepancies in details as an indicator that the computed zenith ionospheric delay using dual-frequency carrier phase measurements is superior to the GIM model whose

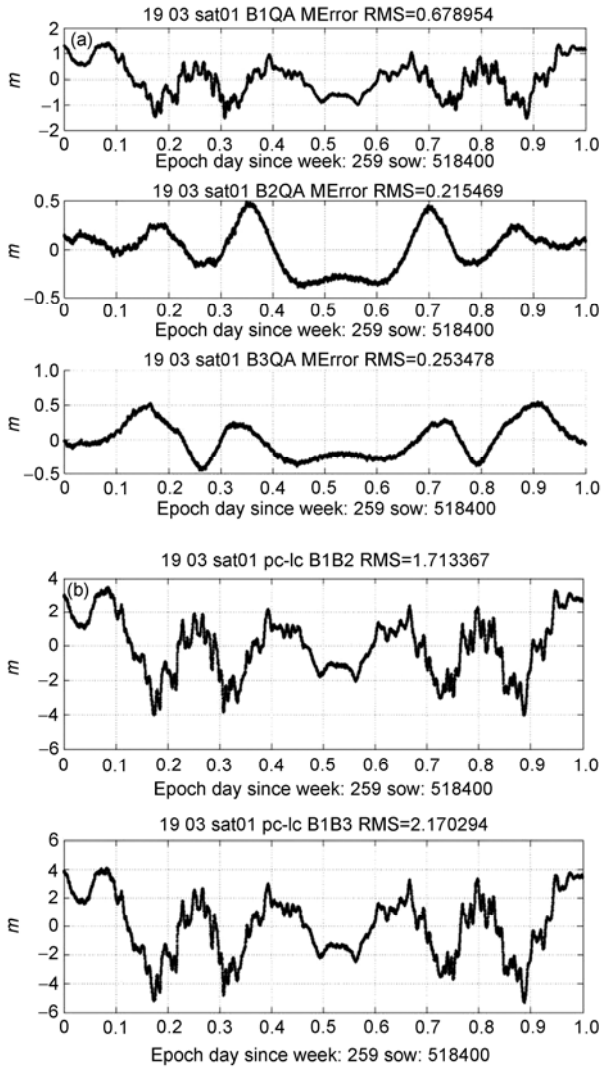

Figure 2 (a) The multipath error of single-frequency pseudorange. The horizontal axis represents observation time (unit: day). The three graphs from top to bottom represent the pseudorange multipath error at B1, B2, and B3 separately. (b) The multipath error of pseudorange ionosphere-free combination. The top and bottom graphs represent the multipath error of the B1-B2 ionosphere-free combination and the B1-B3 ionosphere-free combination.

spatial resolution is not enough for minor variations. However, because of the multipath error of pseudorange measurements, there are significant differences between the computed ionospheric delay using dual-frequency pseudorange combinations and the real ionospheric delay as computed by the carrier phase combinations. The maximum VTEC error introduced by the B1-B2 pseudorange multipath is over 8 TECU (2 m), and the maximum VTEC error introduced by the B1-B3 pseudorange multipath is up to 12 TECU (3 m).

2 Real-time CNMC algorithm

The GPS multipath studies have demonstrated that because

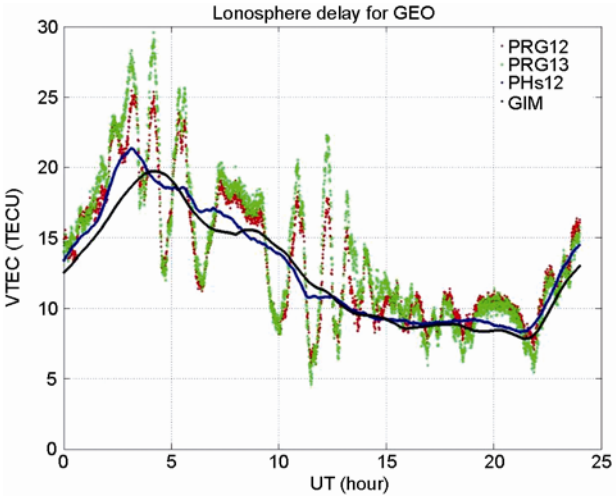

Figure 3 The zenith ionospheric delay using different frequency measurement combinations. The horizontal axis represents a day observing arc (unit: hour), the vertical axis represents VTEC(unit: TECU). The red, green and blue curves represent the computed VTEC using the B1-B2 pseudorange combination, the B1-B3 pseudorange combination and the B1-B2 carrier phase combination, respectively. The black curve represents the VTEC at the corresponding IPP using the GIM model.

of the complex causes and time-varying characteristic of multipath effects, the commonly used error processing technologies such as data modeling and differential treatments are not able to completely eliminate the multipath error [1].

In order to remove the pseudorange noise and multipath errors, a dual-frequency multipath monitor was developed at the WAAS Reference Sites (WRS) [5–9]. Given the different characteristics of China's regional satellite navigation system, a real-time multipath correction algorithm is proposed on this basis in this paper, which is called CNMC (Code Noise and Multipath Correction). This algorithm is used to correct multipath errors and random noise of pseudorange measurements at the master processing station.

Ignoring the carrier phase multipath and random noise, according to the pseudorange and carrier phase observation equations (eqs. (1), (2)), it can be easily verified that the difference between the peudorange and the carrier phase measurements at the same epoch (Code Minus Carrier, CMC) should be nothing but double ionospheric delay, ambiguity combination, hardware interfrequency biases, pseudorange multipath error and random noise. The current epoch ionospheric delay (with ambiguity) can be computed using dual-frequency carrier phase measurements. The basic idea of CNMC is that if the ambiguity combination and hardware biases of code-minus-carrier could be successfully estimated, the multipath errors and random noise of pseudorange measurements would then be separated. A recursive process is used to estimate the ambiguity combination and hardware biases. As a carrier smoothing pseudorange method in essence, the CNMC algorithm relies on continuous cycle-slip-free carrier phase measurements.

Different from the WAAS algorithm used exclusively for GPS satellites, the CNMC algorithm proposed in this paper is mainly applied to GEO satellites of China's regional navigation system. As GEO's geostationary feature ensures continuous measurements, the cycle slips of the carrier phase are relatively rare, so getting better multipath correction performance is expected. Furthermore, in order to meet requirements on real-time and reliability, the algorithm processing strategy must be optimized.

2.1 CNMC algorithm

According to eqs. (1) and (2), the difference between the pseudorange and the carrier phase measurements at the same epoch is as follows:

$$CMC = P - \phi \cdot \lambda = 2\Delta t_{\text{iono}} + \tau_{\text{sat}} + \tau_{\text{rcv}} + M_{\text{P}} + \varepsilon_{\text{P}} - Amb_{\phi}. \quad (8)$$

Therefore,

$$M_{\text{P}} + \varepsilon_{\text{P}} = P - \phi \cdot \lambda - 2\Delta t_{\text{iono}} - \tau_{\text{sat}} - \tau_{\text{rcv}} + Amb_{\phi}. \quad (9)$$

The ionospheric delay (with ambiguity) can be computed using dual-frequency carrier phase measurements. The difference between B1 and B2 carrier phase measurements is given by:

$$\phi_1 \cdot \lambda_1 - \phi_2 \cdot \lambda_2 = \left(\Delta t_{\text{iono\_2}} - \Delta t_{\text{iono\_1}}\right) + b_{12}, \quad (10)$$

where, b_{12} consists of a combination of phase interfrequency biases and the difference of dual frequency ambiguity. In the subsequent estimates, this parameter will be assumed constant during a continuous cycle-slip-free observation arc.

The ionospheric delay estimated at B1 can be written as follows:

$$\begin{aligned}\Delta t_{\text{iono\_1}} &= \frac{f_2^2}{f_1^2 - f_2^2}\left(\phi_1 \cdot \lambda_1 - \phi_2 \cdot \lambda_2 - b_{12}\right) \\ &= k_1\left(\phi_1 \cdot \lambda_1 - \phi_2 \cdot \lambda_2\right) - k_1 \cdot b_{12}. \end{aligned} \quad (11)$$

Similarly, the ionospheric delay estimated at B2 can be given as follows:

$$\begin{aligned}\Delta t_{\text{iono\_2}} &= \frac{f_1^2}{f_1^2 - f_2^2}\left(\phi_1 \cdot \lambda_1 - \phi_2 \cdot \lambda_2 - b_{12}\right) \\ &= k_2\left(\phi_1 \cdot \lambda_1 - \phi_2 \cdot \lambda_2\right) - k_2 \cdot b_{12}. \end{aligned} \quad (12)$$

Replacing the ionospheric delay in eq. (9) with eq. (11), we get eq. (13):

$$\begin{aligned} M_{\text{P}_1} + \varepsilon_{\text{P1}} &= P_1 - \phi_1 \cdot \lambda_1 - 2k_1\left(\phi_1 \cdot \lambda_1 - \phi_2 \cdot \lambda_2\right) \\ &\quad + 2k_1 \cdot b_{12} - \tau_{1\text{sat}} - \tau_{1\text{rcv}} + Amb_{\phi 1} \\ &= P_1 - \phi_1 \cdot \lambda_1 - 2k_1\left(\phi_1 \cdot \lambda_1 - \phi_2 \cdot \lambda_2\right) - \text{Bias}_1. \end{aligned} \quad (13)$$

Multipath equations for B2 and B3 frequencies are not

given in this paper because of the same derivation process. For a certain frequency, the real-time pseudorange multipath correction algorithm is as follows [3]:

To initialize CNMC:

$$\begin{aligned} &\mathrm{Bias}(t_0) = P(t_0) - \phi(t_0)\cdot\lambda - 2\Delta t_{\mathrm{iono}}(t_0), \\ &M_{\mathrm{P}}(t_0) + \varepsilon(t_0) = 0. \end{aligned} \tag{14}$$

After initialization, the estimate of CMC biases and real-time multipath corrections are updated as follows:

$$\begin{aligned} \mathrm{Bias}(t_N) &= \mathrm{Bias}(\mathrm{t}_{N-1}) + \frac{P(t_N)}{N} - \frac{1}{N}(\phi(t_N)\cdot\lambda + \mathrm{Bias}(t_{N-1}) \\ &\quad + 2\Delta t_{\mathrm{iono}}(t_{\mathrm{N}}), \\ M_{\mathrm{P}}(t_N) + \varepsilon_{\mathrm{P}}(t_N) &= P(t_N) - \phi(t_N)\cdot\lambda - 2\Delta t_{\mathrm{iono}}(t_N) \\ &\quad - \mathrm{Bias}(t_N), \end{aligned} \tag{15}$$

where, t_N represents the Nth epoch time from the initialization and N is the number of updates in the recursive process. Specifically, when a cycle slip is detected, a new initialization and recursive process must be restarted.

2.2 Multipath correction effects using CNMC algorithm

According to the pseudorange multipath eq. (7), the multipath RMS of original pseudorange measurements and the error RMS of multipath-corrected measurements using CNMC are computed to assess the effectiveness of this algorithm.

Table 1 lists the multipath RMS of original pseudorange and the error RMS of multipath-corrected measurements using CNMC at B1. The results of 15 receivers and 5 satellites are given, and the observing arc is one day. In Table 1, sat1, sat2 and sat3 are GEO satellites and sat4 and sat5 are IGSO satellites. The last line in Table 1 represents the improvement percentage for each satellite. As can be seen from Table 1, the multipath errors are significantly reduced by using CNMC, and the multipath corrections for GEO satellites are more effective than that for IGSO satellites. To better illustrate the reduction of multipath errors by using CNMC, we use the histogram below to show the error RMS of the pseudorange measurements for GEO 1 (Figure 4). The black column represents the RMS before multipath correction, while the white column represents the RMS after multipath correction.

The multipath errors in three frequency pseudorange measurements of two receivers are shown in Figure 5. Note these two receivers are located thousands of km apart. The grey curves describe the multipath errors of the pseudorange measurements before multipath correction and the black curves represent the errors in the multipath-corrected measurements by using CNMC.

It can also be seen from Figure 5 that there are CNMC re-initializations. Since it always costs a period of time to successfully estimate the ambiguity combination after a new initialization, the convergence time varies with the multipath amplitude at the re-initialization epoch. Generally, the convergence time is about 2–3 hours, with a residual multipath error of several centimeters after the convergence.

The three graphs from top to bottom represent the pseudorange multipath errors at B1, B2 and B3 respectively. The grey and black curves represent the multipath errors of the original pseudorange measurements and the multipath-corrected measurements respectively.

Table 1 Comparison of pseudorange multipath error RMS at B1 before/after CNMC (unit: m)

Receiver	Sat1		Sat2		Sat3		Sat4		Sat5	
	Before	After	Before	After	Before	After	Before	After	Before	After
01	0.065	0.009	0.123	0.042	0.114	0.039	0.072	0.050	0.072	0.050
02	0.165	0.053	0.091	0.032	0.261	0.065	0.136	0.083	0.098	0.083
03	0.164	0.083	0.186	0.098	0.286	0.112	0.113	0.097	0.109	0.097
04	0.135	0.043	0.075	0.026	0.281	0.142	0.150	0.093	0.203	0.093
05	0.156	0.088	0.119	0.050	0.245	0.084	0.176	0.104	0.206	0.104
06	0.720	0.201	0.112	0.028	–	–	0.329	0.143	0.204	0.143
07	0.507	0.310	0.203	0.074	–	–	0.235	0.129	0.214	0.129
08	0.165	0.056	0.071	0.026	0.558	0.232	0.136	0.082	0.137	0.082
09	0.197	0.047	0.077	0.025	0.816	0.310	0.129	0.072	0.105	0.072
10	0.199	0.100	0.402	0.214	0.277	0.133	0.200	0.056	0.167	0.056
11	0.150	0.077	0.239	0.106	0.245	0.140	0.222	0.124	0.124	0.124
12	0.418	0.143	0.239	0.167	0.622	0.194	0.137	0.140	0.373	0.140
13	0.149	0.070	0.245	0.104	0.125	0.060	0.082	0.060	0.104	0.060
14	0.127	0.056	0.182	0.080	0.142	0.034	0.149	0.054	0.089	0.054
15	0.200	0.043	0.497	0.097	0.270	0.076	0.241	0.123	0.210	0.123
Mean	0.234	0.092	0.191	0.078	0.326	0.125	0.167	0.094	0.161	0.094
	60.68%		59.16%		61.66%		43.70%		41.61%	

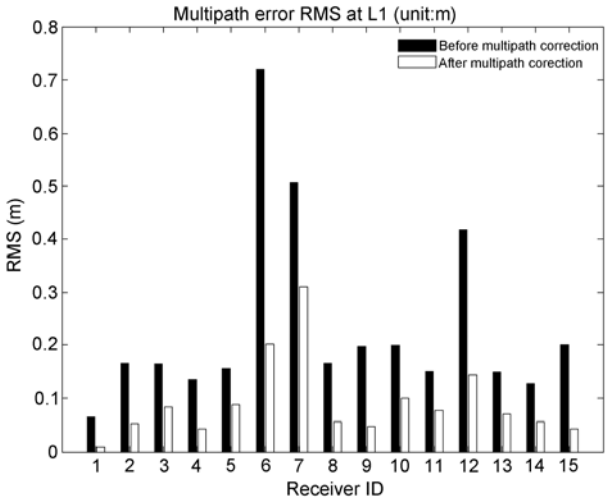

Figure 4 CNMC multipath correction effect histogram.

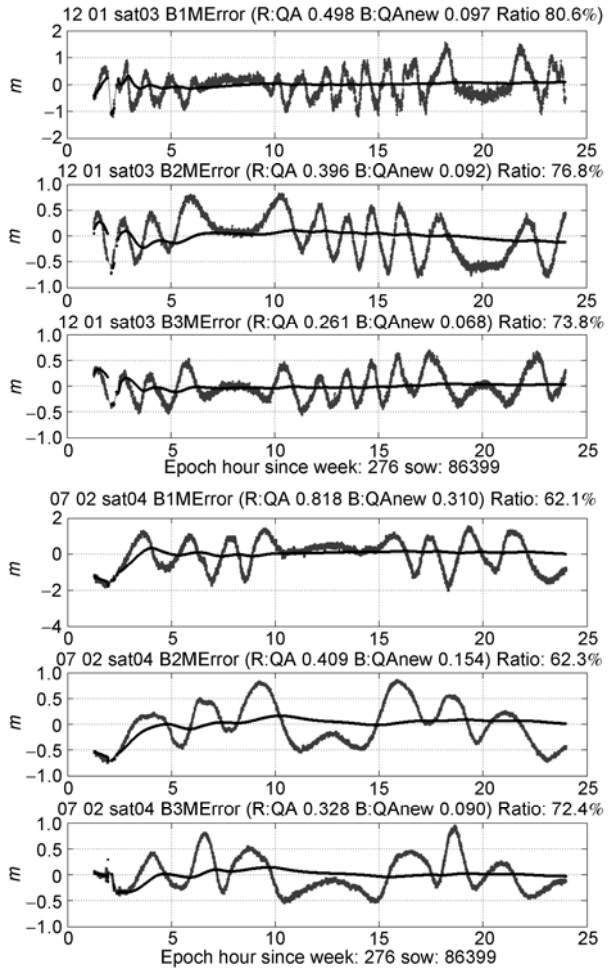

Figure 5 The original and residual multipath errors.

2.3 CNMC algorithm for positioning

Based on China's regional satellite navigation system, the station's position and receiver clock error can be computed after obtaining satellite ephemeris and clock error parameters from the broadcasting navigation message. The position result will be converted to the station centric coordinate system and compared with the station coordinate (as measured by GPS, with an accuracy of better than 10 cm) to assess the positioning error.

The single point positioning error depends on the user equivalent range error (UERE) and the position dilution of precision (PDOP) [10]. PDOP is associated with the constellation geometry of satellites and UERE is the summation of measurement errors and the broadcasting navigation message errors. The latter is the major factor influencing the current UERE accuracy. The UERE can be computed as follows:

$$\begin{aligned}\mathrm{UERE} = P - \left|\boldsymbol{R}^{\mathrm{sat}} - \boldsymbol{R}_{\mathrm{rcv}}\right| - \Delta t_{\mathrm{revclk}} + \Delta t_{\mathrm{satclk}} \\ - \Delta t_{\mathrm{trop}} - \Delta t_{\mathrm{iono}} - \Delta t_{\mathrm{cor}} - \tau_{\mathrm{sat}} - \tau_{\mathrm{rcv}},\end{aligned} \tag{16}$$

where, P is a pseudorange measurement, $\boldsymbol{R}_{\mathrm{rcv}}$ is the known receiver position vector, $\boldsymbol{R}^{\mathrm{sat}}$ is the calculated satellite position vector using the broadcast ephemeris, $\Delta t_{\mathrm{satclk}}$ is the calculated satellite clock error using the broadcast clock error parameters, τ_{sat} is the satellite time delay obtained from the broadcast navigation message and Δt_{trop} and Δt_{cor} are the errors that can be computed with models. Dual frequency users can remove the ionospheric delay Δt_{iono} by using dual-frequency measurements. The position error is approximately equal to the product of UERE and PDOP [11].

For the constellation of 3 GEO plus 3 IGSO satellites, the position error of a dual-frequency user is given in Figure 6. Figure 6(a) shows the positioning errors using original pseudorange measurements, while Figure 6(b) shows the positioning errors after CNMC multipath correction with the same navigation messages. The dashed, dotted and solid lines represent the East-West (longitude), South-North (latitude) and vertical position accuracy in the top graph. The middle graph shows 3D position error and the bottom graph is the PDOP at each epoch. Because GEO satellites are located above the equator, the stronger constraint on East-West results in higher position accuracy on the East-West direction than the other two. As can be observed from Figure 6, the reduction of random noise in pseudorange measurements is significant with the application of CNMC. As shown in Figure 6(a), the vertical and 3D position errors in the time period from hour 4 to hour 5 (UT) are relatively large because of the larger multipath errors in the original pseudorange measurements. Statistical results show that 66.9% of position errors are over 5 m within this period, and 18.2% of position errors are even over 10 m. After correcting multipath errors with CNMC, within the same period, only 0.8% of position errors are over 5 m. In contrast, because the main reason sources of the larger position errors from the beginning to the first hour are orbit errors and clock errors during this period, the position errors in this period are only slightly improved in Figure 6(b) after the

multipath errors correction. Overall, the East-West position accuracy is improved from 1.31 m to 0.94 m by using the CNMC algorithm, the South-North position accuracy is improved from 2.62 m to 2.29 m, and the vertical position accuracy is improved from 4.25 m to 3.05 m. After correcting multipath errors, the 3D position accuracy is improved from 5.16 m to 3.94 m. The mean of the PDOP value is 5.67 with six hours observation arc. The discontinuity of the PDOP curve corresponds to the different IGSO satellites entry or exit.

For a dual-frequency user, the RMS of position error is given in Table 2, with E, N and U representing the East-West, South-North and vertical directions respectively. As can be seen from the table, the CNMC algorithm enables a signification improvement in position accuracy.

Real data analysis indicates that for high-precision differential users, the multipath error from the measurement section has become an important factor to the user position accuracy after eliminating the broadcast ephemeris and clock parameter error by using the equivalent clock correction. After correcting multipath errors by using CNMC, there is a more significant improvement in the user position accuracy compared with the ordinary user (see separate article).

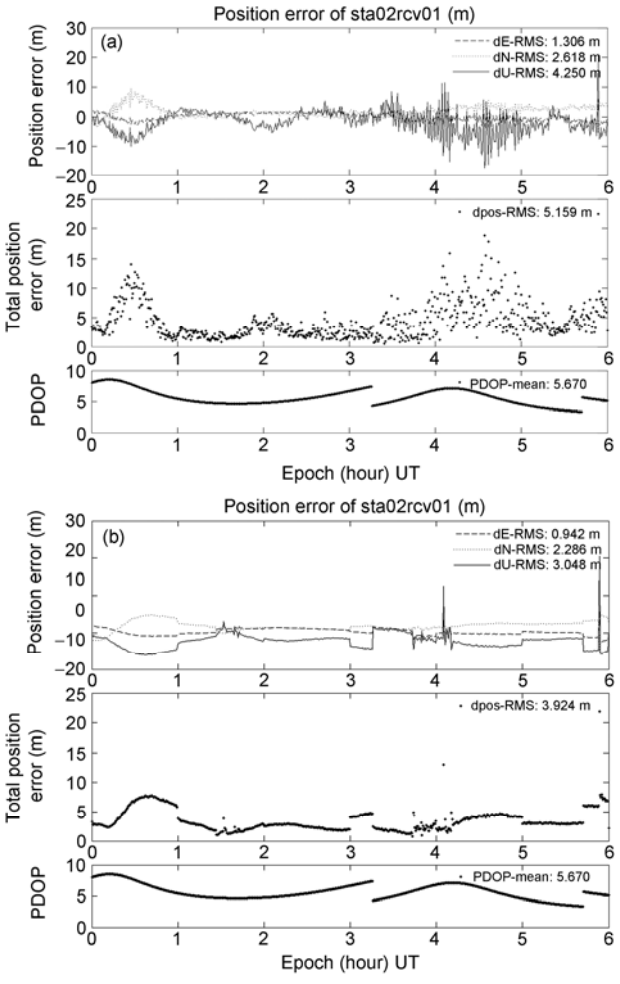

Figure 6 (a) Dual-frequency user position error with the original pseudorange measurements; (b) dual-frequency user position error after CNMC multipath correction. The dashed, dotted and solid lines represent the East-West, South-North and vertical position error in the top graph, respectively. The black curve in the middle graph represents the 3D position error and the black curve in the Bottom graph represents the PDOP.

Table 2 The dual-frequency position error RMS using original and multipath correction measurements (unit: m)

	E	*N*	*U*	Total
Before CNMC	1.31	2.62	4.25	5.16
After CNMC	0.94	2.29	3.05	3.94

3 Problems and discussions

Experiments have verified that the multipath reduction of pseudorange measurements is significant when using the real-time CNMC algorithm, but the effectiveness of CNMC is subject to the continuity of carrier phase measurements. The reason is that dual-frequency carrier phase measurements are needed to compute the ionospheric delay and to estimate the ambiguity combination and hardware biases in the code-minus-carrier combinations.

Theoretically, the CNMC correction will be the true multipath with the assumption the multipath can be modeled as a zero mean variable. Otherwise, the bias of the multipath mean value will be introduced into the correction. At the *N*th (*N*>1) recurrence epoch, the current multipath correction is given in the next equation, which needs to be added to the original pseudorange measurement as a multipath correction.

$$M_{\mathrm{P}} = M_{\mathrm{P}}(t_{\mathrm{N}}) + \frac{M_{\mathrm{P}}(t_1) + M_{\mathrm{P}}(t_2) + \cdots + M_{\mathrm{P}}(t_{N-1})}{N-1} = M_{\mathrm{P}}(t_N) + M_{\mathrm{erro}}. \quad (17)$$

Although the analysis of real data has shown that the mean value of one-day multipath errors is about zero, with a bias of several centimeters, the mean of one-hour multipath errors may be up to 1 m, which means a new bias will be introduced to the pseudorange measurements after correcting the multipath errors. For user positioning calculations, the same part of the bias of each satellite will be absorbed into the receiver clock error, but the different part of the bias of each satellite will influence the user range error (URE), and degrade the user position accuracy.

The effectiveness of the real-time CNMC algorithm is subject to the data quality. When the data are continuous and stable, the process from initialization to recursive convergence is smooth, therefore good multipath correction performance will be achieved. But if there are frequent cycle slips, data interruptions or more outliers of a receiver's measurements, the algorithm strategy is designed to re-initialize at these epochs, so the multipath correction performance of this receiver's measurements will be poor in this case.

The multipath errors and real-time multipath corrections for a GEO satellite are shown in Figure 7(a). The multipath errors and real-time multipath corrections for an IGSO satellite are shown in Figure 7(b). The light gray curve represents the post-processed multipath errors according to eq. (7) with high accuracy ambiguity resolution, which is not available for real-time processing. The dark gray curve is the real-time multipath correction at each epoch using CNMC, which needs a recursive period to estimate the ambiguity combination, so there are differences (black curves in the right graph) between the light and dark gray curves. The black curve represents the error M_{erro} after correcting the multipath error. Ideally, the multipath error and the real-time correction at an epoch is the same, so the dark gray curve and the light gray curve should coincide perfectly, and the black curve should be a straight line with zero value. But according to eqs. (14) and (17), the multipath correction at the initialization epoch is zero. And in the following recursive process, the multipath correction contains the mean value of cumulative multipath errors except for the true error at each epoch, which results in a difference between the correction and true value. But with the convergence of the recursive process, the deviation tends to be zero. As shown in Figure 7, the dark gray curves tend to overlap with the light gray curves, and the black curves tend to be zero. In Figure 7(a), there is a breakpoint in the right-top graph which is caused by the re-initialization when the algorithm detects the interrupted data over 60 s. It is the same case in the other graphs in the right part of Figure 7(a).

Solar activity will enter the peak period in the year of 2012. Strong solar storms and geomagnetic storms may cause frequent loss of carrier phase lock. In this case, the reliability and stability of the CNMC algorithm may need further experiments.

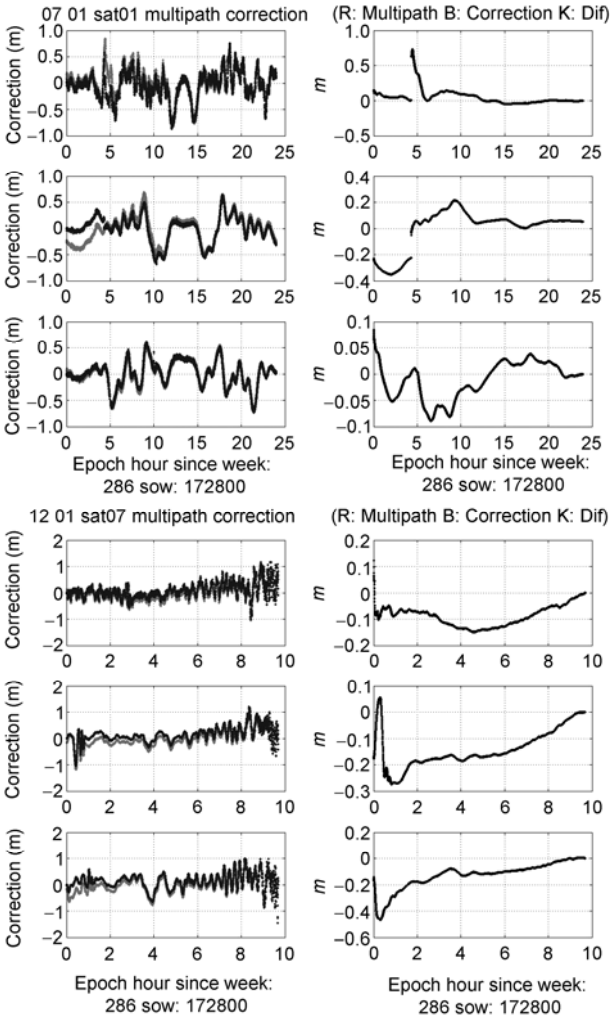

Figure 7 (a) GEO multipath error and correction; (b) IGSO multipath error and correction. The light gray curves represent the multipath errors of the original pseudorange measurements. The dark gray curves represent the real-time multipath corrections, and the black curves show the residual errors. The top, middle and bottom graphs show the errors at B1, B2 and B3.

4 Conclusions

To correct multipath errors of GEO /IGSO pseudorange measurements of China's regional navigation system, the multipath error of carrier phase measurements is first analyzed in this paper using real data. The analysis indicates that the peak-to-peak multipath error of carrier phase ionosphere-free combination is less than 3 cm with an RMS less than 1cm. Both are two orders of magnitude smaller than that of pseudorange measurements.

A real-time multipath correction algorithm is proposed in this paper, which is called the CNMC algorithm. The algorithm is based on the phase smoothing pseudorange algorithm which was developed in WAAS to reduce multipath error. We have improved and optimized the algorithm and successfully applied it to positioning calculations to improve the performance of China's regional navigation system.

The analysis of real data indicates that the multipath error level is reduced from 0.5 m to 0.15 m by using this algorithm, and 60% of GEO multipath errors and 42% of IGSO multipath errors are successfully corrected with CNMC. In order to ensure the system reliability, the algorithm is designed to re-initialize when there is a new cycle slip or abnormal data occurs. So frequent cycle slips or more abnormal data will reduce the effectiveness of the CNMC algorithm. When the data are continuous and stable, the residual error is less than 0.1 m after correcting the multipath. Positioning experiments are performed with a constellation of 3GEO plus 3IGSO satellites. For dual-frequency users the East-West position accuracy is improved from 1.31 m to 0.94 m by using the CNMC algorithm, the South-North position accuracy is improved from 2.62 m to 2.29 m, and the vertical position accuracy is improved from 4.25 m to 3.05 m. After correcting multipath errors, the three-dimen-

sional position accuracy is improved from 5.16 m to 3.94 m.

The authors would like to thank the anonymous reviewers for their thoughtful reviews, Professor WU Bin and Professor PING JinSong for their technical helps. We would also like to thank LIU Li, CHANG ZhiQiao, GUO Rui, SU RanRan and FENG XiaoChao for their comments and assistances. This work was supported by the National High Technology Research and Development Program of China (863) (Grant Nos. 2009Z12A324 and 2009AA12Z328), the National Natural Science Foundation of China (Grant Nos. 10703011, 11073047 and 11033004), and the Science and Technology Commission of Shanghai (Grant No. 06DZ22101).

1 Feng X C, Jin G P. Experimentation and analysis of multipath in code-ranged by GNSS receiver. Geomat Inform Sci Wuhan Univ, accepted
2 Schempp T, Burke J, Rubin A. WAAS benefits of GEO ranging. In: Proceedings of ION-GNSS 21st. International Technical Meeting, Savannah, GA., Sept. 12–15, 2008
3 Zhou S S, Hu X G, Wu B, et al. Orbit determination and time synchronization for a GEO/IGSO satellite navigation constellation with regional tracking network. Sci China Phys Mech Astron, 2011, 54(6): 1089–1097
4 Dean B. On the treatment of noise and conspiring bias in dual-frequency global navigation satellite systems. The Dissertation for Doctoral Degree. Ohio: Ohio University, Electrical Engineering, 2010. http://etd.ohiolink.edu/multiview.cgi/ohiou1262040825/ohiou-1262040825.pdf
5 van Graas F. Wide Area Augmentation System Research and Development, Final Report. Prepared under Federal Aviation Administration Research Grant 01-G-016, February 2004. http://www.tc.faa.gov/logistics/grants/pdf/2001/01-G-016.pdf
6 Shallberg K, Shloss P, Altshuler E, et al. WAAS measurement processing, reducing the effects of multipath. In: Proceedings of the 14th International Technical Meeting of the Satellite Division of The Institute of Navigation, September, 2001, Salt Lake City, Utah
7 Phelts R E, Walter T, Akos D, et al. Range biases on the WAAS geostationary satellites. In: Proceedings of the Institute of Navigation National Technical Meeting, January 2004, San Diego, CA
8 Dean B, van Graas F, Skidmore T. Statistical characterization of composite protection levels for GPS. GPS Solut, 2010, 15(3): 263–273
9 Karl S, Fang S. WAAS measurement processing: Current design and potential improvements. In: Proceedings of IEEE/ION PLANS 2008, Monterey, CA, May 2008. 253–262
10 Liu J Y. GPS Navigation and Positioning Principles and Methods. Beijing: Science Press, 2003